Microcavities based on multimodal interference

Björn Maes, Mihai Ibanescu, John D. Joannopoulos

Dept. of Physics, Center for Materials Science and Engineering, Research Laboratory of Electronics, Massachusetts Institute of Technology, 77 Massachusetts Avenue, Cambridge 02139, Massachusetts, USA

bjorn.maes@ugent.be

Peter Bienstman, Roel Baets

Photonics Research Group, Ghent University, St.-Pietersnieuwstraat 41, 9000 Ghent, Belgium

Abstract: We describe intricate cavity mode structures, that are possible in waveguide devices with two or more guided modes. The main element is interference between the scattered fields of two modes at the facets, resulting in multipole or mode cancelations. Therefore, strong coupling between the modes, such as around zero group velocity points, is advantageous to obtain high quality factors. We discuss the mechanism in three different settings: a cylindrical structure with and without negative group velocity mode, and a surface plasmon device. A general semi-analytical expression for the cavity parameters describes the phenomenon, and it is validated with extensive numerical calculations.

OCIS codes: (230.5750) Resonators; (240.6680) Surface plasmons.

References and links

1. K.J. Vahala, "Optical microcavities," Nature **424,** 839-846 (2003).
2. M. Ibanescu, S.G. Johnson, D. Roundy, Y. Fink, and J.D. Joannopoulos, "Microcavity confinement based on an anomalous zero group-velocity waveguide mode," Opt. Lett. **30,** 552–554 (2005).
3. M. Hammer, "Resonant coupling of dielectric optical waveguides via rectangular microcavities: the coupled guided mode perspective," Opt. Comm. **214,** 155–170 (2002).
4. M. Hammer, "Total multimode reflection at facets of planar high-contrast optical waveguides," Journ. Lightw. Tech. **20,** 1549–1555 (2002).
5. S.G. Johnson, S. Fan, A. Mekis, and J.D. Joannopoulos, "Multipole-cancellation mechanism for high-Q cavities in the absence of a complete photonic band gap," Appl. Phys. Lett. **78,** 3388–3390 (2001).
6. P. Bienstman and R. Baets, "Optical modelling of photonic crystals and VCSELs using eigenmode expansion and perfectly matched layers," Opt. Quantum Electron. **33,** 327–341 (2001).
7. A. Farjadpour, D. Roundy, A. Rodriguez, M. Ibanescu, P. Bermel, J.D. Joannopoulos, S.G. Johnson, and G. Burr, "Improving accuracy by subpixel smoothing in FDTD," Opt. Lett. **31,** 2972-2974 (2006).
8. A. Karalis, E. Lidorikis, M. Ibanescu, J.D. Joannopoulos, and M. Soljačić, "Surface-plasmon-assisted guiding of broadband slow and subwavelength light in air," Phys. Rev. Lett. **95,** 063901 (2005).
9. H.A. Haus, *Waves and fields in optoelectronics* (Prentice-Hall, 1984).
10. M. Ibanescu, S.G. Johnson, D. Roundy, C. Luo, Y. Fink, and J.D. Joannopoulos, "Anomalous dispersion relations by symmetry breaking in axially uniform waveguides," Phys. Rev. Lett. **92,** 063903 (2004).
11. P.P.P. Debackere, P. Bienstman, and R. Baets "Adaptive Spatial Resolution: Application to Surface Plasmon Waveguide Modes," accepted for publication in Opt. Quantum Electron.
12. T.P. White, L.C. Botten, R.C. McPhedran, and C.M. de Sterke, "Ultracompact resonant filters in photonic crystals," Opt. Lett. **28,** 2452–2454 (2003).

#80543 - $15.00 USD Received 28 Feb 2007; accepted 22 Mar 2007; published 7 May 2007

1. Introduction

Optical microcavities with high quality factors and small modal volumes are used in a wide range of applications such as low-threshold lasers, optical filters, nonlinear optics and cavity quantum electrodynamics [1]. Therefore it is important to know which mechanisms may lead to efficient confinement, and in which systems they are applicable.

Here we focus on a class of microcavities that can be described as a section of a waveguide. The properties of the guided waveguide modes and their reflection at the facets determine the cavity characteristics. The existence of high-quality cavity modes in waveguides with a zero group velocity point was shown in [2]. In the present paper we give a more in-depth description of these cavity modes. We show that the mechanism is very similar to the phenomenon in [3, 4], and we point out the connection with the multipole cancelation mechanism [5]. In [3, 4] one describes how the interference between multiple modes may lead to high facet reflections. We give a simple semi-analytical description of this phenomenon by examining the round-trip matrix of the cavity. There is a correlation between the possible reflection enhancement and the interaction between the modes. A zero group velocity point in the dispersion relation of a waveguide creates two modes that are intimately related. Therefore, these modes are good candidates to exploit the cavity mechanism.

The variation of length and frequency generates a rich variety of cavity modes, more than initially expected in [2]. The parameters of these modes are precisely described by the model, which gives a straightforward expression for the eigenvalues of the (half) round-trip matrix. By approximating this formula it is easy to obtain insight into the modal trends. The discussion is supported by detailed numerical simulations based on eigenmode expansion [6] and finite-difference time-domain (FDTD) calculations [7].

The phenomenon is described using three structures. First, we employ the zero group velocity cylindrical structure proposed in [2]. We reach clear insights into the cavity mechanism, and at the same time we validate the new approaches. Second, we study the same structure, but at a wavelength with two normal (i.e. positive group velocity) guided modes. The same mechanism appears, however the dispersion and reflection characteristics are quite different. Third, we examine a surface plasmon cavity device, based on a recently proposed waveguide with a zero group velocity point [8]. Again, clear resonances are available, however the details differ.

The paper is organized as follows. First we describe the semi-analytical formulas and the numerical methods used. Then, in the main part, we discuss in sequence the previously mentioned three structures. Finally we group the conclusions.

2. Semi-analytic and numerical modeling

The class of devices under study is quite general and is depicted in Fig. 1(a). The center of the cavity is a waveguide system with two guided modes. Therefore the properties of the cavity modes are determined by the dispersion and reflection properties of these waveguide modes. We consider symmetric cavities, thus with two equal facets.

Because we deal with two guided modes, the reflection and propagation properties are described by 2×2-matrices. The reflection and propagation matrix are denoted by R and P, respectively. As usual, a resonance or cavity mode is achieved if the imaginary part of an eigenvalue of the round-trip matrix (or, because of symmetry, half-trip matrix) is zero. The half-trip matrix is given by $P \times R$. In case of resonance, the quality factor Q of the cavity mode is determined by the magnitude of its eigenvalue, or, more precisely, by how close the half-trip eigenvalue is to ± 1. If the waveguide modes have the same group velocity magnitude $|v_g|$ (ir-

#80543 - $15.00 USD Received 28 Feb 2007; accepted 22 Mar 2007; published 7 May 2007

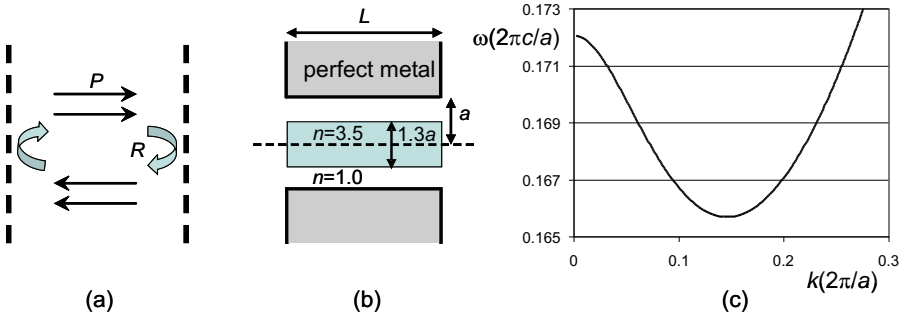

Fig. 1. (a) General picture of a system with two circulating modes. (b) Schematic of the cylindrical structure. The dashed line is the axis of the cylinder. (b) Dispersion of the HE_{11} mode.

respective of the sign), we obtain [9]

$$Q = \frac{\omega_r L}{|v_g|\,(1-|\lambda|^2)}. \tag{1}$$

Here, ω_r is the resonance frequency of the cavity mode and L is the length of the waveguide. λ is the eigenvalue of the half-trip matrix, so

$$P \times R \begin{bmatrix} c_0 \\ c_1 \end{bmatrix} = \lambda \begin{bmatrix} c_0 \\ c_1 \end{bmatrix}, \tag{2}$$

with c_0 and c_1 the complex eigenvector components corresponding with the eigenvalue λ, which are normalized so $|c_0|^2+|c_1|^2=1$. In the case of waveguide modes with different group velocity magnitudes v_g^0 and v_g^1, the factor v_g in Eq. 1 is replaced by

$$v_g^{average} = |v_g^0||c_0|^2 + |v_g^1||c_1|^2. \tag{3}$$

To obtain the eigenvalue λ we need to construct the half-trip matrix. We assume a time dependence $\exp(i\omega t)$. Then, for two positive v_g modes, we get the matrix for propagation over a length L:

$$P = \begin{bmatrix} \exp(-ik_0L) & 0 \\ 0 & \exp(-ik_1L) \end{bmatrix}, \tag{4}$$

with k_0 and k_1 the waveguide mode propagation constants of mode 0 and mode 1, respectively. We always assume k_0 and k_1 positive (and $k_0 > k_1$), so for a negative v_g mode we need to adjust the sign in the propagation matrix. E.g. if mode 0 has negative v_g we have to use $\exp(ik_0L)$, as the power fluxes of both modes need to be in the same direction. The waveguide modes in the examples have negligible propagation losses, but including losses does not change the equations. The complex reflection matrix describes the modal reflection properties at a facet:

$$R = \begin{bmatrix} r_{00} & r_{01} \\ r_{10} & r_{11} \end{bmatrix}, \tag{5}$$

where, because of reciprocity, $r_{01} = r_{10}$. In the next equations it is sometimes convenient to work with average and difference values, so: $k_0 = k+\Delta, k_1 = k-\Delta$. Likewise for the reflection matrix: $r_{00} = d+\delta, r_{11} = d-\delta$.

#80543 - $15.00 USD Received 28 Feb 2007; accepted 22 Mar 2007; published 7 May 2007

Now, we can readily note the eigenvalues of the half-trip matrix $P \times R$. There are slight differences in the equation for the three structures discussed in the following sections, as the elements of the propagation matrix depend on the positive or negative v_g character of the modes. In the case of the example in the next section mode 0 has positive v_g and mode 1 has negative v_g. Then we obtain:

$$\lambda = \exp(-i\Delta L)\left[d\cos(kL) - i\delta\sin(kL) \pm \sqrt{(-id\sin(kL) + \delta\cos(kL))^2 + r_{01}^2}\right]. \qquad (6)$$

In the case of two positive v_g modes (as in section 4) we have to interchange k and Δ in the previous equation. Finally, in the case where mode 0 has negative v_g and mode 1 has positive v_g (as in section 5), we have to interchange i with $-i$ in equation 6. The previous equation gives us a comprehensive picture of the cavity modes. The imaginary part determines which combinations of frequency and length L give rise to a resonant mode. Then the real part indicates how strong the resonance is, through the quality factor in equation 1.

The previous description is semi-analytical, because we need modeling methods to get the propagation constants and the reflection matrix. For this purpose we use CAMFR, a freely available eigenmode expansion simulation tool [6] (http://camfr.sourceforge.net). As CAMFR is an efficient frequency domain code we quickly obtain these parameters at each frequency of interest. These values are then employed to study the eigenvalues and quality factors with the previous equations, for different cavity lengths L. Some of the resonant modes have been simulated with MEEP, a freely available finite-difference time-domain (FDTD) code, in order to validate the semi-analytical model [7] (http://ab-initio.mit.edu/wiki/index.php/Meep). Good agreement has been obtained, as we present below, showing that the modal description is sufficient.

3. Cylindrical cavity: negative group velocity mode

We study the same cylindrical structure in this section and the next. However, we discuss different frequency regions and modes of different angular symmetry. A schematic is shown in Fig. 1(b), it is the same device as in [2]. It was shown that this structure gives rise to a zero v_g point in the dispersion relation of the HE_{11} mode [10]. We plot this dispersion in Fig. 1(c). The geometry is useful as a model for similar phenomena that can appear in omniguide or photonic bandgap structures [2, 10].

To find cavity modes we scan the (ω, L)-space. In the frequency region with two interacting waveguide modes (mode 0 with positive v_g and mode 1 with negative v_g) we find high-Q cavity resonances. This is presented in Fig. 2(a). Some of these Q-peaks (dark blue dots in Fig. 2(a)) were discussed in [2]. Now however we find additional modes. The origin of the extra modes is elucidated in Fig. 2(b). In this graph we put a dot each time a resonance is obtained, thus each time the imaginary part of λ becomes zero, regardless of the size of the real part. In this way we clearly see the connection between the resonances. The branches are grouped in pairs. Each pair corresponds to a certain resonance order. Each branch in a pair corresponds to a symmetry (node versus antinode in the middle of the cavity). Only the lowest order pair (lower left in Fig. 2(b), dark blue dots) was described in [2]. Note that the agreement between the semi-analytic mode expansion approach and FDTD is indicated in Fig. 2, which validates the approach.

The field distribution of some modes is shown in Fig. 3, together with the far field on- and off-resonance of a cavity mode. Clearly the multipole cancelation effect is at work, as described in [5]. At a high-Q resonance the radiation pattern changes: there are extra nodal lines, see Fig. 3(b), as the lowest order multipole is canceled. This gives proof of a bimodal mechanism: Both waveguide modes are prominent in the cavity. At the facets they reflect but radiate some

#80543 - $15.00 USD Received 28 Feb 2007; accepted 22 Mar 2007; published 7 May 2007

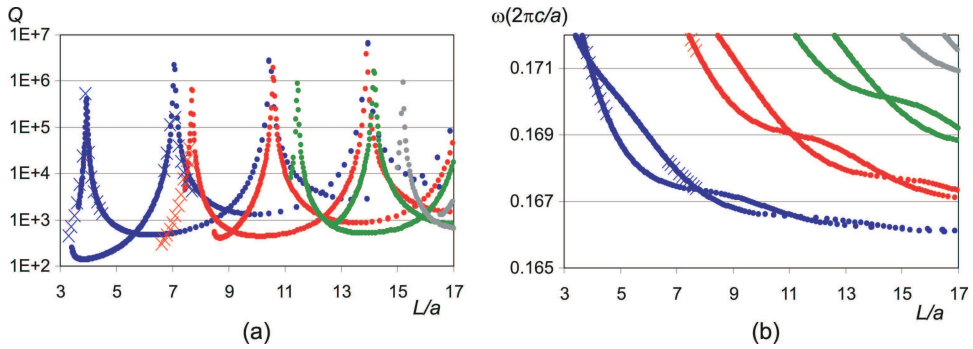

Fig. 2. (a) Q versus L of the resonances. Dots are data points from mode expansion (CAMFR), crosses present results from FDTD (MEEP). (b) ω versus L for the same cavity modes.

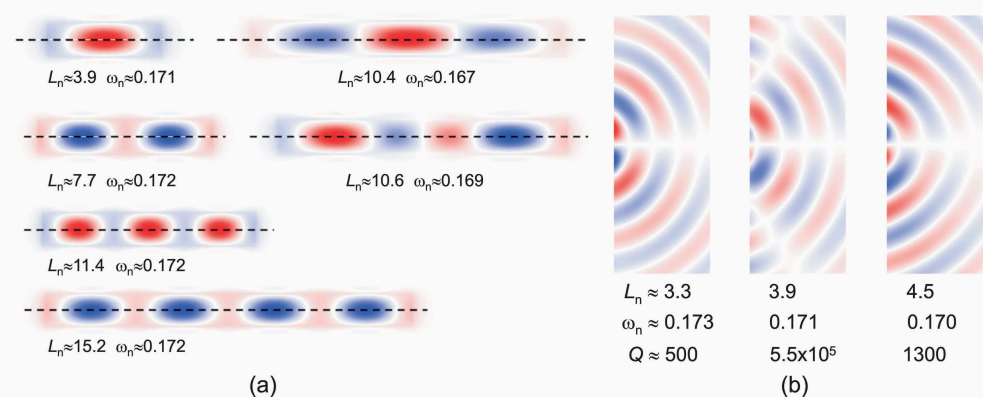

Fig. 3. (a) Field plot of some resonances. The electric field along ϕ is shown. L_n and ω_n are L/a and $\omega \times (a/2\pi c)$, respectively. (b) Far-field on- and off-resonance. The magnetic field along the direction of the axis is shown. The cavity is located to the left of these plots.

energy into the space adjacent to the cavity. This radiation can be described as a superposition of multipoles. At certain cavity lengths and frequencies two conditions are fulfilled: there is a phase resonance (imaginary part of λ is zero), and the important lowest order multipole contribution of the modes cancel each other (leading to a real part of λ close to one, meaning low losses). When these conditions are satisfied we obtain a high-Q cavity. This mechanism was also at work in the two-dimensional square structures of [3] and [4].

To gain insight into the particular frequencies and lengths of resonance we study the eigenvalue equation more closely. It turns out that for each example in this paper we can make approximations to obtain the main trends of the resonances. The approximations are made via the reflection matrix. The magnitudes of the elements of this matrix for the current example are shown in Fig. 4. For a large range of frequencies it is clear that the off-diagonal element is larger than the diagonal ones, thus $|r_{01}| > |r_{00}|, |r_{11}|$ (or $|r_{01}| > |d|, |\delta|$). In that case the magnitude of the eigenvalues (from Eq. 6) is approximated by:

$$|\lambda|^2 \approx |r_{01}|^2 \pm 2\cos(kL)\mathrm{Re}(r_{01}d^*) \mp 2\sin(kL)\mathrm{Im}(r_{01}\delta^*), \tag{7}$$

where Re (Im) is the real (imaginary) part, and * means complex conjugate. This expression implies that the magnitude of λ (at constant L) is only a weakly-varying function of the fre-

#80543 - $15.00 USD
Received 28 Feb 2007; accepted 22 Mar 2007; published 7 May 2007

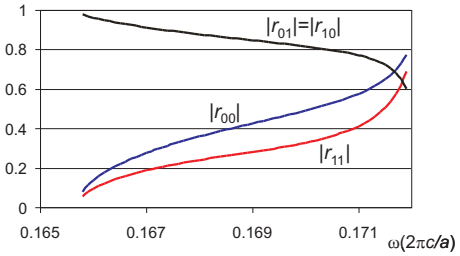

Fig. 4. Magnitudes of the reflection matrix elements for the cylindrical structure with the negative group velocity mode.

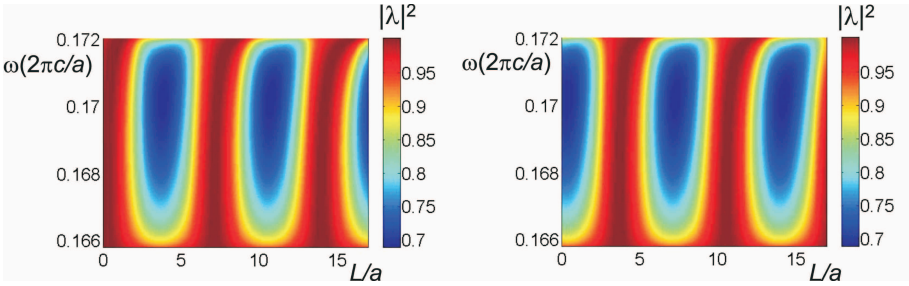

Fig. 5. Magnitude squared of the two eigenvalues for the cylindrical structure in the frequency range with a negative group velocity mode.

quency. In function of L (at constant ω) the maxima of $|\lambda|^2$ are separated by π/k or $3.4a$. Note that in this example k corresponds with the zero v_g-point. The exact $|\lambda|^2$ values are plotted in Fig. 5; we indeed see vertical lines of magnitude extrema, separated horizontally by $3.4a$.

For the phase resonance we can simplify a bit further and obtain:

$$\lambda \approx \pm r_{01} \exp(-i\Delta L). \tag{8}$$

This means that the L-difference between two pairs or resonance orders (at a certain frequency) is given by π/Δ. Thus, if we approach the zero v_g-point, Δ goes to zero, and the distance between pairs becomes infinite. This explains the trends of the branches in Fig. 2(b).

Combining the magnitude and the imaginary part describes the cavity modes. If a magnitude maximum (the red vertical ribbons in Fig. 5) coincides with a phase resonance one obtains a mode with a very high Q. The previous also elucidates the longitudinal length scale π/k provided by the zero v_g-point, which was only partly explained in [2].

4. Cylindrical cavity: positive group velocity modes

Here we study the same cylindrical structure as in the previous section, but at higher frequencies and with angular momentum zero (which means an angular dependence $\cos(m\phi)$ with $m = 0$, as opposed to $m = 1$ in the previous example). The dispersion of the TE modes (only one electric field component, along ϕ) is plotted in Fig. 6. We examine the frequency region with two guided modes between $\omega = 0.4$ and $0.6(2\pi c/a)$, indicated in the figure, and we note that both modes have a positive v_g.

Scanning the (ω, L)-space we obtain resonances again, which are shown in Fig. 7. These graphs look different than in the previous example. However, study of the far-field (not shown) and the Q-peaks shows again that multipole cancelation is at work. Therefore, the bimodal

#80543 - $15.00 USD Received 28 Feb 2007; accepted 22 Mar 2007; published 7 May 2007

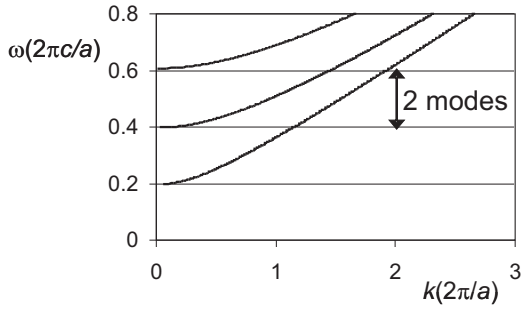

Fig. 6. Dispersion of the TE modes with angular momentum zero in the cylindrical structure. The frequency region with two guided modes is indicated.

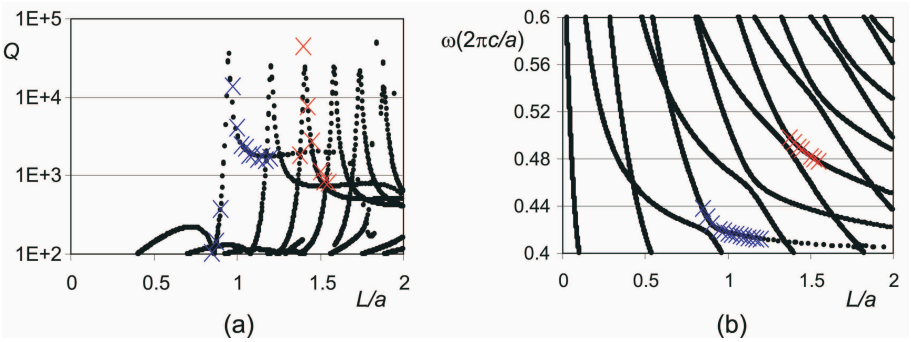

Fig. 7. (a) Q versus L of resonances. Dots are data points from mode expansion (CAMFR), crosses present checks with FDTD (MEEP). (b) ω versus L for the cavity modes in the cylindrical structure with two positive v_g waveguide modes.

resonance mechanism is equivalent, but we need to examine the dissimilarity with the previous section. The field patterns for some resonances are depicted in Fig. 8(a).

The differences in the trends are explained by an analysis of the eigenvalue. The reflection matrix is shown in Fig. 8(b), and it is quite different from Fig. 4 for the previous example. Here, we see that $|r_{00}|, |r_{11}| > |r_{01}|$ (and also $|d| > |r_{01}|$ and $|\delta| > |r_{01}|$). In this case the magnitude of λ is approximated by:

$$|\lambda|^2 \approx |d \pm \delta|^2 \pm \mathrm{Re}\left(\frac{c^2 (d^* \pm \delta^*) \exp(\pm i \Delta L)}{-id \sin(\Delta L) + \delta \cos(\Delta L)} \right). \tag{9}$$

This means we obtain an extremum of $|\lambda|^2$ if the denominator in this equation becomes small, or (approximately) if $\tan(\Delta L) \approx -|\delta/d|$, which gives a period (at constant frequency) of π/Δ. As the frequency increases, we note that both $|\delta/d|$ and Δ decrease, so the maximum of $|\lambda|^2$ moves to larger L, as shown in Fig. 9.

The phase branches in Fig. 7(b) clearly present two different trends. Analysis shows that, away from the main interaction points (these are the anti-crossings, where in this case the high-Q values are reached), the branches are approximated by $\lambda_+ \approx r_{00} \exp(-ik_0 L)$ and $\lambda_- \approx r_{11} \exp(-ik_1 L)$, respectively. An anti-crossing switches the trends of the curves between λ_+ and λ_-. A crossing indicates that the branches correspond to a different symmetry (node or antinode in the middle of the cavity). In between anti-crossings the curves follow $\mathrm{Im}(\lambda_+) = 0$ or $\mathrm{Im}(\lambda_-) = 0$, respectively. The latter indicates e.g. that the branch veers off to higher L, as

#80543 - $15.00 USD Received 28 Feb 2007; accepted 22 Mar 2007; published 7 May 2007

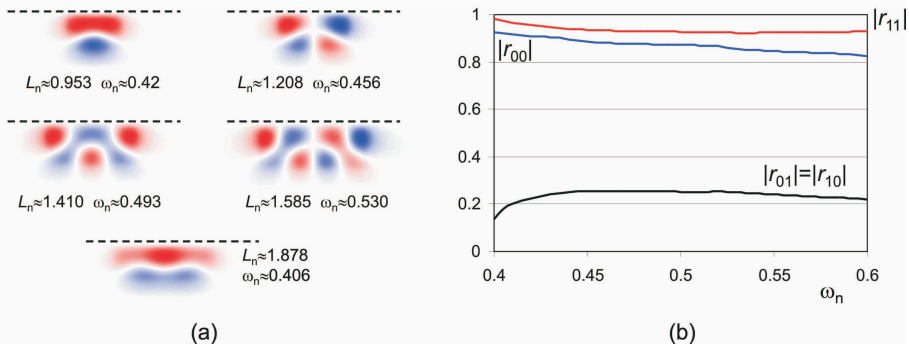

Fig. 8. (a) Field plot of some resonances. The electric field along ϕ is shown; only one half is presented. L_n and ω_n are L/a and $\omega \times (a/2\pi c)$, respectively. (b) Magnitudes of the reflection matrix elements for the cylindrical structure in the frequency range with two positive group velocity modes.

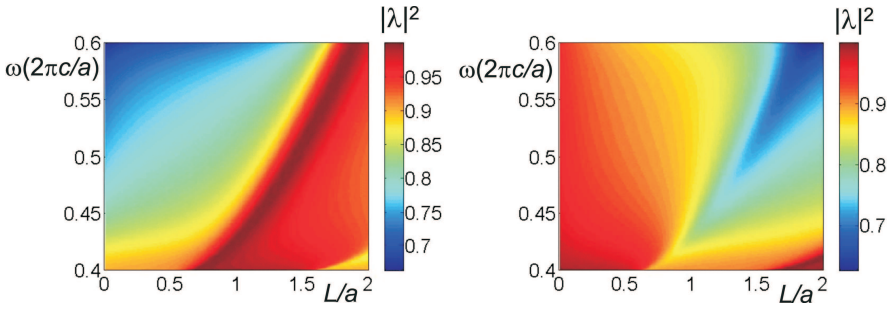

Fig. 9. Magnitude squared of the two eigenvalues for the cylindrical structure in the frequency range with positive group velocity modes.

the frequency nears the cut-off for mode 1. Furthermore, the distance (at constant frequency) between branches is $2\pi/k_0$ or $2\pi/k_1$, respectively.

Overlaying amplitude and phase (Fig. 9 and Fig. 7(b)) we see that the high-Q cavities appear at the anti-crossing regions in Fig. 7(b), as previously noted.

5. Plasmonic cavity

In this section we construct a cavity mode by exploiting a zero v_g-point in the dispersion of a plasmonic waveguide. This dispersion relation appears in a waveguide consisting of metal with a narrow dielectric layer on top, as presented in [8]. The two-dimensional, non-cylindrical geometry we study is shown in Fig. 10(a). We use a metal-dielectric-metal structure, so there are two semi-infinite metal slabs, with a dielectric strip in between. The cavity is defined by the narrow dielectric sections with higher index ($n = \sqrt{2}$), the rest is air ($n = 1$). For the metal we use the permittivity $\varepsilon = 1 - \omega_p^2/\omega^2$, with ω_p the plasmon frequency.

The waveguide is designed such that the center section (with the high-index parts) has two guided modes in a certain frequency range, whereas the outside sections (to the left and to the right) have one guided, more conventional, plasmonic mode. These dispersion relations are shown in Fig. 10(b). Note that we only consider modes with symmetry such that the electric field tangential to the plane indicated with the dashed line in Fig. 10(a) is zero. Furthermore, we use TM-polarization, thus with one magnetic field component perpendicular to this figure.

#80543 - $15.00 USD Received 28 Feb 2007; accepted 22 Mar 2007; published 7 May 2007

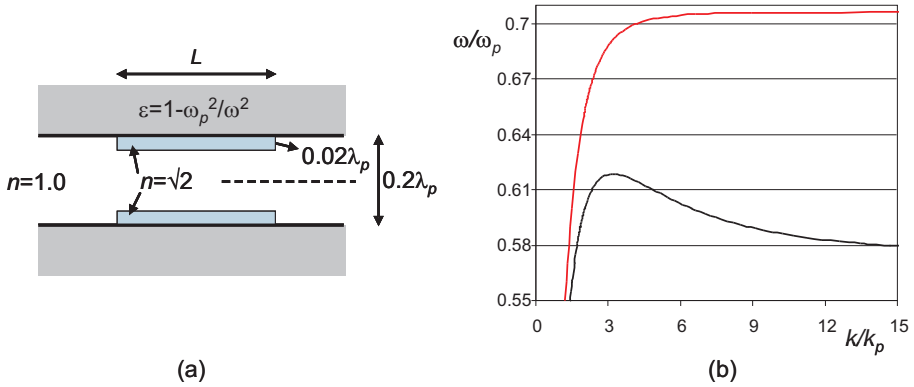

Fig. 10. (a) Schematic of the two-dimensional, non-cylindrical plasmon structure. (b) Dispersion of the central waveguide (black), and of the outside waveguides (red).

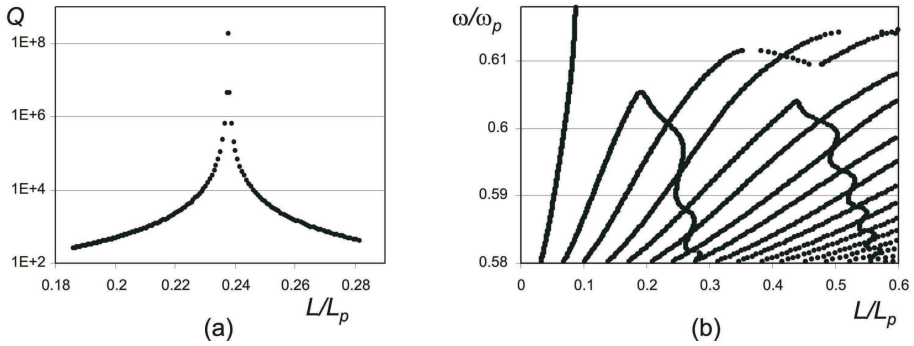

Fig. 11. (a) Q versus L of a resonance. Data calculated with mode expansion (CAMFR). (b) ω versus L for the plasmonic cavity.

The eigenmode solver we use has been adapted to deal with plasmonic modes, see [11].

The structure differs from the previous examples in that there is no open space to the left and right of the cavity. Therefore, there is no loss into (multipole) radiation, but only through the guided mode in the outside sections. However, high-Q cavities can exist through cancelation of the contributions to this loss mode. Thus, the bimodal mechanism of the previous sections remains crucial and largely unchanged. The situation bears similarity e.g. to the setting of [12] with directional couplers.

A resonance peak for the quality factor is presented in Fig. 11(a). For clarity only one peak is shown. A depiction of the field at this resonance is given in Fig. 12(a). Note that we obtain very high quality factors, as there is only one mode that provides a loss channel, and needs to be canceled. The phase resonance portrait is shown in Fig. 11(b). Again the portrait looks different than for the other examples.

The analysis starts from the reflection matrix, shown in Fig. 12(b). Away from the direct neighborhood of the zero v_g-point we can assume that $|r_{00}| > |r_{01}|$ and $r_{11} \approx 0$ (or $d \approx \delta$ and $|d| > |r_{01}|$). We note furthermore that the reflection matrix is approximately real. In that case the magnitude of the largest eigenvalue approximates to:

$$|\lambda_+|^2 \approx r_{00}^2 + 2r_{01}^2 \cos(2kL) + \frac{r_{01}^4}{r_{00}^2}. \tag{10}$$

#80543 - $15.00 USD
Received 28 Feb 2007; accepted 22 Mar 2007; published 7 May 2007

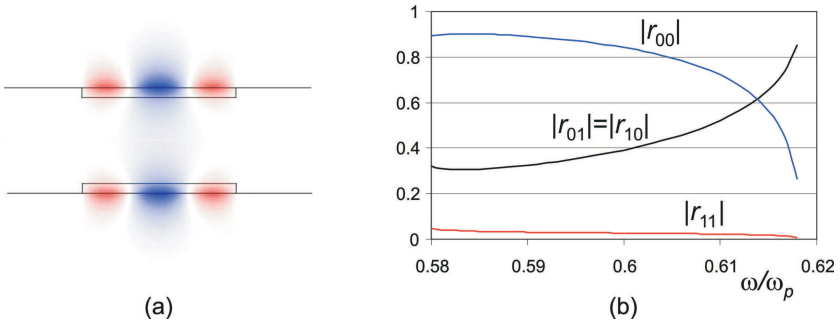

Fig. 12. (a) Depiction of the magnetic field at the peak of the resonance shown in Fig. 11(a) ($L = 0.238L_p$ and $\omega = 0.601\omega_p$). (b) Magnitudes of the reflection matrix elements for the plasmonic structure.

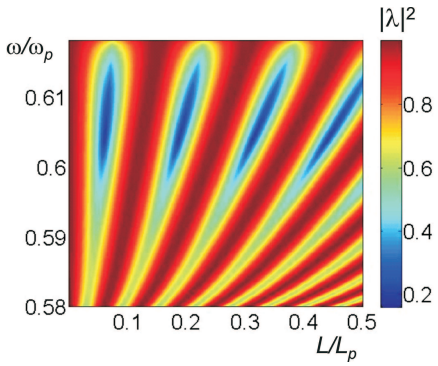

Fig. 13. Numerically calculated magnitude squared of an eigenvalue for the plasmonic structure.

This means a period (at constant frequency) of π/k. Indeed, we see this trend in the numerical results of Fig. 13: If the frequency increases then k decreases and the period increases.

For the phase picture we obtain that $\lambda_+ \approx r_{00}e^{ik_0L}$. There is resonance if $\mathrm{Im}(\lambda_+)$ equals zero, so $L = m\pi/k_0$, with m a positive integer. This agrees with the main lines in the portrait of Fig. 11(b). The curly lines originating close to the zero v_g-point, and the anti-crossings, are not captured by this analysis, as the approximations no longer apply, or because they belong to λ_-.

6. Conclusion

The interplay of two modes in a cavity gives rise to high quality resonances. In the case of open space cavities they instigate the multipole cancelation mechanism. In the case of losses through guided modes, the losses are annulled via Fabry-Pérot type interference. We give a detailed description of these mechanisms through three examples. Although the mechanism is similar, the reflection matrix and the resulting resonance parameters look quite different. We show that modes coupled through a zero group velocity point are well suited to realize these resonances. The main ingredient seems to be a significant coupling between the waveguide modes. A recently proposed plasmon waveguide is exploited for this effect. The analysis provides a clear path to design and gain insight into novel cavity devices.

#80543 - $15.00 USD Received 28 Feb 2007; accepted 22 Mar 2007; published 7 May 2007

Acknowledgments

BM and PB acknowledge postdoctoral fellowships from the Funds for Scientific Research - Flanders (FWO-Vlaanderen). This work was supported in part by the MRSEC Program of the National Science Foundation under award number DMR 02-13282.

#80543 - $15.00 USD Received 28 Feb 2007; accepted 22 Mar 2007; published 7 May 2007